The International Journal of Advanced Manufacturing Technology (2023) 127:4123–4132
https://doi.org/10.1007/s00170-023-11731-4

ORIGINAL ARTICLE

Comparative study of corrosion susceptibility and microstructural effects on AA7075-T6 aluminum alloys under different heat treatments

Fatima Ezzohra El Garchani[1] · **Moulay Rachid Kabiri**[1]

Received: 28 March 2023 / Accepted: 1 June 2023 / Published online: 23 June 2023

Abstract

Al–Zn–Mg–Cu alloys of the 7xxx series have superior strength in their maximum aging condition (T6) compared to other age-hardenable aluminum alloys. Here, a comparative study of the corrosion susceptibility of AA7075-T6 aluminum alloys was performed under two heat treatments. A 5% NaCl salt solution at a temperature of 40 °C and neutral pH in the salt spray chamber was used to evaluate the microstructure and corrosion behavior of the aluminum alloy. The samples underwent two heat treatments; one included quenching solution using heat treatment at 475 °C, and the other included aging for 4 days. Several tests such as Vickers hardness test, optical microscope, SEM, as well as tensile test were used to study the characteristics of this alloy. The surface characteristics, including refined microstructure and residual stresses, were characterized, and their effect on localized corrosion was studied. The maximum strength value of the sample that underwent aging decreased by 24.85%, yet an increase was noticed for elongation of 18%. Pitting was more severe for the quenching treatment than for the aging and control treatments. This could be attributed to the formation of fine ή-phase precipitates that are fully coherent or partially coherent; the aging treatment improves the corrosion resistance due to the smaller size of the corrosion product after the specimen was etched in different areas.

Keywords AA7075 · Corrosion · SEM · Tensile test · Microhardness

1 Introduction

Applications for high-strength aluminum alloys are common in the construction, automotive, aerospace, and defense industries. Alloy AA7075 is a high-strength aluminum alloy from the 7000 family that is based on the Al-Zn-Mg system. Mg and Zn combine to generate strengthening precipitates such as $MgZn_2$ and Mg_3Zn, which enhance the alloy's mechanical qualities. The "phase" (semi-coherent $MgZn_2$) that precipitates inside the grain and the "phase" (incoherent $MgZn_2$) that precipitates along the grain boundary are what give it its strength [1–3]. A 7075 aluminum alloy is utilized in aircraft applications due to its high strength-to-density ratio, corrosion resistance, and high fracture toughness.

Aluminum structures used in aircraft suffer from pitting corrosion, a degrading mechanism that compromises their dependability, toughness, and integrity [4–10]. The $MgZn_2$ strengthening particles (g0 and g phases) that contribute to the high strength of 7xxx alloys during T6 temper aging dissolve as a result of solution heat treatment [11, 12]. When the alloy is rapidly quenched from the solution treatment temperature to ambient temperature, the dissolution of $MgZn_2$ strengthening particles produces a matrix enriched with solute atoms like Zn, Mg, and Cu, which results in the presence of supersaturated solid solutions [13–15]. Alloys composed of Al, Zn, Mg, and Cu, such as AA7075, are susceptible to severe localized corrosion like pitting, intergranular corrosion, and spalling [16].

Heat treatment, which modifies the alloy's microstructure to produce ideal mechanical properties, has a significant impact on these alloys' sensitivity [10, 17]. Al–Zn–Mg–Cu alloy applications in the aerospace sector are complicated by some microstructures' limited resistance to localized corrosion. Pitting is supposed to happen to airplane parts when the aircraft is idle in between flights; it is unlikely to happen while the aircraft is in flight because of the freezing temperatures at high altitudes. Pitting is caused by either local matrix dissolution or intermetallic compound dissolution as a result of

✉ Fatima Ezzohra El Garchani
f.ezzohra.elgarchani@gmail.com

[1] Laboratory of Energetic, Materials and Sustainable Development, University Moulay Ismail, ENSAM, 50500 Meknes, Morocco

galvanic interaction between the intermetallic compound and the matrix [18].

Among the Al–Zn–Mg–Cu alloys, AA7075 has received the most attention because the aerospace sector uses it so frequently. Intermetallic complexes and reinforcing particles can be found in the microstructure of AA7075 [10, 12]. Interaction between alloying elements and alloy impurities causes intermetallic compounds to develop during casting and ingot homogenization [16]. They range in size from 1 to 20 µm. The most prevalent intermetallic compounds in AA7075 are Al_7Cu_2Fe and $(Al, Cu)_6$ (Fe, Cu), while Mg_2Si intermetallic compounds are less common [17, 19]. Intermetallic compounds go through phase transitions and change shape during ingot homogenization, but solution heat treatment and alloy aging have little effect on them [20, 21].

Research has shown the importance of studying the effects of heat treatments on aluminum alloy AA7075. N. M. Siddesh Kumar et al. have shown that precipitation-hardening alloys of the 7XXX family increase tensile strength, fracture toughness, and hardness while reducing ductility, elongation, toughness, and stress corrosion cracking. Retrogression and re-aging, with microstructure, precipitates comparable to those in the T6 condition and excessive aging in the T7 condition, are used to arrest stress corrosion cracking [22]. Marta Orlowska et al. showed that the size of MgZn2 precipitates within the microstructure increased following artificial aging, and changes in the chemical composition of the matrix improved corrosion resistance. Due to the position of precipitates at grain boundaries, which did not strengthen the material, variations in mechanical strength as a function of aging temperature were not significant [23]. Gang Wang et al. methodically studied precipitates and their development on AA7075-H18 alloy sheets during the solution setting process. Insoluble particles, such as Al23CuFe4 and Mg2Si, and soluble particles, such as -MgZn2, were found to be uniformly distributed in the H18 alloy sheet. The solution temperature should be set between 470 and 505 °C to ensure complete dissolution and avoid overheating [24].

The strength of AA7075 alloy is enhanced by various heat treatments. The T6 heat treatment applied to this alloy is one of the most important means of improving the alloy's mechanical properties, both by solid solution heat treatment and aging treatment [25]. The potential advantages of the heat treatment effect in terms of mechanical and microstructural qualities, as well as corrosion behavior, have only been briefly examined in a few studies. As a result, the purpose of this paper is to offer a thorough examination in this direction. This work represents an attempt to clarify the effect of heat treatment on the corrosion resistance and mechanical properties of AA7075-T6 aluminum alloys under two different treatments (quenching and aging). This study is based on SEM–EDS and optical microscope as well as microhardness and tensile tests to study the evolution of the behavior of this alloy.

2 Materials and methods

2.1 Material

Aluminum alloy 7075-T6 (AA7075-T6) is widely used in engineering. This alloy has good mechanical properties, such as a high specific strength comparable to that of high-strength steel. It offers the possibility of significant weight reduction, which is vital in certain applications [26]. The chemical composition of the studied alloy AL 7075-T6 is shown in Table 1.

2.2 Methods

2.2.1 Salt spray test

Use an ISO 9227 salt spray container for spraying salt on the samples in line with ASTM B117, which is an industry standard. The temperature of the container was maintained at 40 °C, and the salt mist solution was 5.0 w% sodium chloride with a neutral pH. The metal was exposed to 40 cycles for 3 h each.

2.2.2 Heat treatment

The heat treatments undergone by the AA7075-T6 alloy are presented in the following table (Table 2).

2.3 Micrography

2.3.1 Optical microscopy

Measurements of phase and substructure were performed using an OLYMPUS BX60 optical microscope. (OM). Before being incised for 15 s with Keller's solution, the samples were polished to 400, 600, 800, 1000, and 1200, then with 6-µm diamond paste, and finally to micron. (190 ml water, 2 ml hydrofluoric acid, 3 ml hydrochloric acid, and 5 ml nitric acid).

2.3.2 Scanning electron microscope (SEM)

Using the JSM-IT500HR model, the structure of intermetallic particulates was examined during different heat treatment stages both before and after corrosion.

Table 1 Chemical compositions of AA 7075-T6

Element	Zn	Mg	Cu	Fe	Si	Mn	Al
Composition%	6.2	2.0	1.7	0.5	0.4	0.1	Bal

Table 2 Heat treatment conditions of aluminum alloys 7075-T6

Heat treatment	Temperature and holding time	Cooling medium	Temperature and holding time
AA7075-T6 B	475 °C 40 min	Cold water	_____
AA7075-T6 C	475 °C 40 min	Cold water	Ambient temperature 4 days

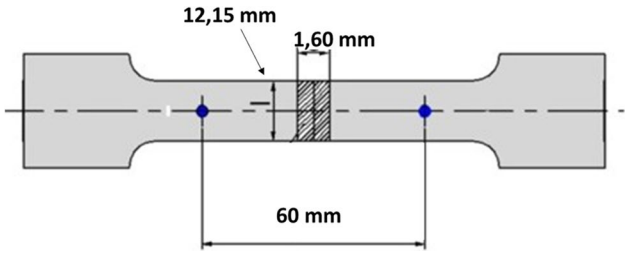

Fig. 1 Aluminum alloy 7075-T6 tensile test specimen

2.4 Characterization

2.4.1 Microhardness

Vickers microhardness testing was performed on each sample to evaluate its tensile properties. The sample is polished from 400 to 1200 grain, stopping at 6 µm and then measured with a forced weight of 100 g for 15 s. Hardness measures each sample at least ten times to determine the typical Vickers hardness.

2.4.2 Tensile test

The 1.60-mm-thick AA 7075-T6 substance was used in the study shown in Fig. 1. Tension experiments were carried out on an Instron Zwick 50KN universal testing apparatus to evaluate the yield strength (YS), ultimate tensile strength (UTS), and elongation to failure (% EL). The test was carried out at room temperature 21 °C at a 50 ± 5% humidity and crosshead speed of 1.5 mm/min in accordance with ASTM B557 [27]. The 0.2% proving stress, UTS, and % EL were determined using the stress–strain diagrams.

3 Results and discussion

3.1 Morphology of aluminum alloys

3.1.1 Temperature effect on the microstructure of AA7075-T6

The optical microscopy results for the heat-treated samples at 100 magnification are shown in Fig. 2.

The morphology of the grains of the alloys was studied by observation using an optical microscope after etching the surface with Keller's reagent, which allows highlighting, the presence of the coarse intermetallic precipitates, and the intermetallic particles. The alloy is heated to a temperature higher than the solvus temperature (475 °C) for 40 min, a sufficient time to reach thermodynamic equilibrium and thus obtain a total solution of the solute atoms. Then, the quenching operation (rapid cooling of the alloy in cold water) prevents the decomposition of the solid solution with the formation of coarse equilibrium precipitates of the η-phase, which is shown in image (b). A solute supersaturated solid solution is obtained where the solute atoms are randomly positioned at the nodes of the face-centered cubic lattice of the aluminum (this is referred to as a substitutional

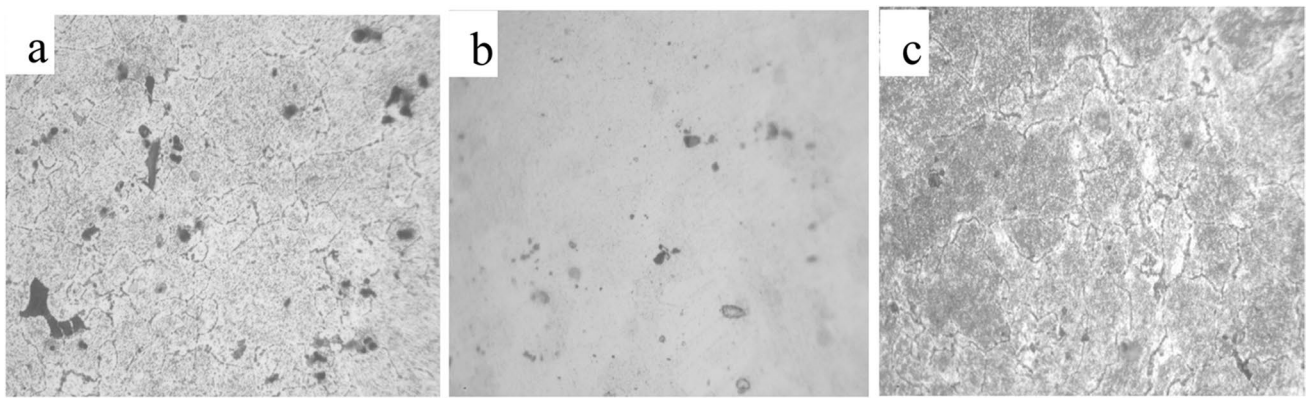

Fig. 2 Micrographs of material AA7075-T6. (**a**) Blank sample alloy. (**b**) Sample of tempering. (**c**) Sample of aging at 100 magnification

solid solution). Image (c) depicts the smaller GP areas disappearing during the maturation of the alloy. Scanning electron microscopy observations coupled with EDS analysis represented by Figs.(3)and (4)showed the nature of the particle types.

Figures (3)and (4) display the results from the EDS analysis and scanning electron microscopy respectively. The SEM studies for the 7075-T6 alloys in their unprocessed condition (picture a) have shown the existence of three coarse intermetallic particles with different morphologies and chemical compositions. Additionally, there are mixed intermetallic particles, which are composed of several precipitates with various chemical characteristics and have separate phases. The Al-Cu-Mn type of intermetallic particle is the first and most abundant type. These precipitates are extensively dispersed throughout the surface of the 7075-T6 alloys and have an erratic form. The second type of particle found in alloy 7075-T6 is also asymmetrical in shape, occasionally taking the shape of rods. They mostly consist of Al, Mg, and Zn. Their composition can be identified as MgZn2 phases by EDS analysis. These particles are real, according to other authors [28]. The brightest zones, which are abundant in Al, Fe, Si, and Mn, correlate to intermetallic particles, according to quantitative EDS analysis. Inside the matrix and close to the grain boundaries, intermetallic particles are visible [29]. The alloy in image (b) has undergone rapid cooling; at this point, a supersaturated solid solution has been created, which accounts for the formation of coarse equilibrium precipitates of the phase in the microstructure. We also note that the distribution of this new phase is heterogeneous. According to the EDS results for image (c), the microstructure contains MgZn2 precipitates; the four points can be regarded as Zn-rich regions. The alloy's strength has been improved most noticeably by the second phase precipitates. In the second phase of the AA7075-T6 alloy's structure, precipitates such Al7Cu2Fe, Al2CuMg, and MgZn2 are produced, according to a prior study [30]. Adeyemi Dayo Isadare et al., explained the formation of MgZn2 microsegregations during progressive solidification of aluminum alloy 7075 due to the redistribution of Mg and Zn solutes, but this phenomenon was suppressed during rapid solidification. However, the microsegregations formed during progressive cooling are dissolved to form a homogeneous phase during the quenching period of heat treatment operations. The age-hardening heat treatment operation resulted in the formation of small, dispersed, and finely uniform precipitates of MgZn2 in the aluminum matrix, while large grains of the MgZn2 phase were formed in the aluminum matrix after the annealing heat treatment operation [31]. Due to the aging treatment's role in demonstrating the material's durability, the second phase (MgZn2) precipitates are generated in the structure [32–34]. The hardening precipitates are formed and distributed throughout the matrix via proper heat treatment: supersaturated solid solution followed by aging. The principal precipitation sequence that dominates hardening in most commercially used 7XXX alloys is presented in Eq. (1):

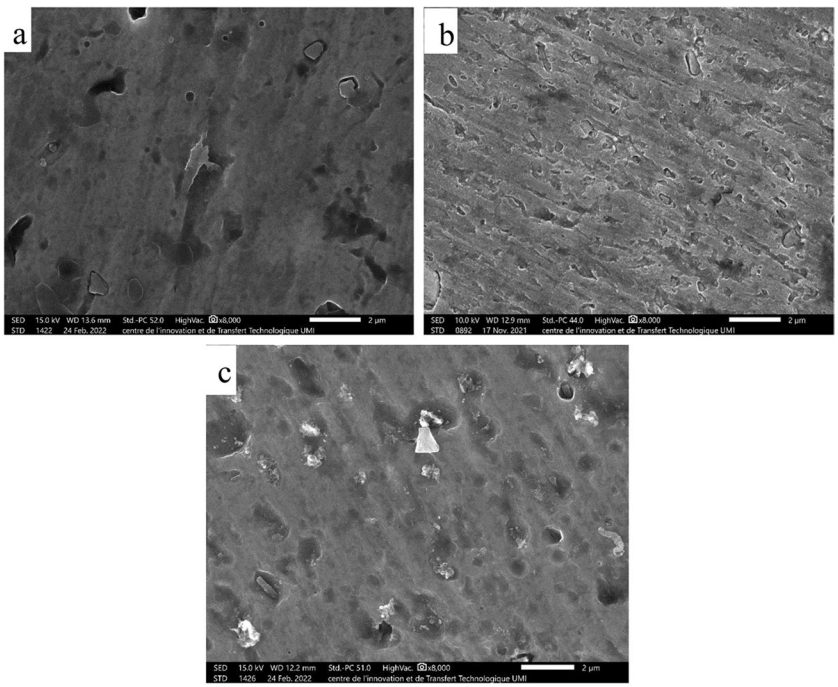

Fig. 3 SEM photomicrograph of alloy AA7075-T6. (**a**) Blank sample alloy. (**b**) Sample of tempering. (**c**) Sample of aging

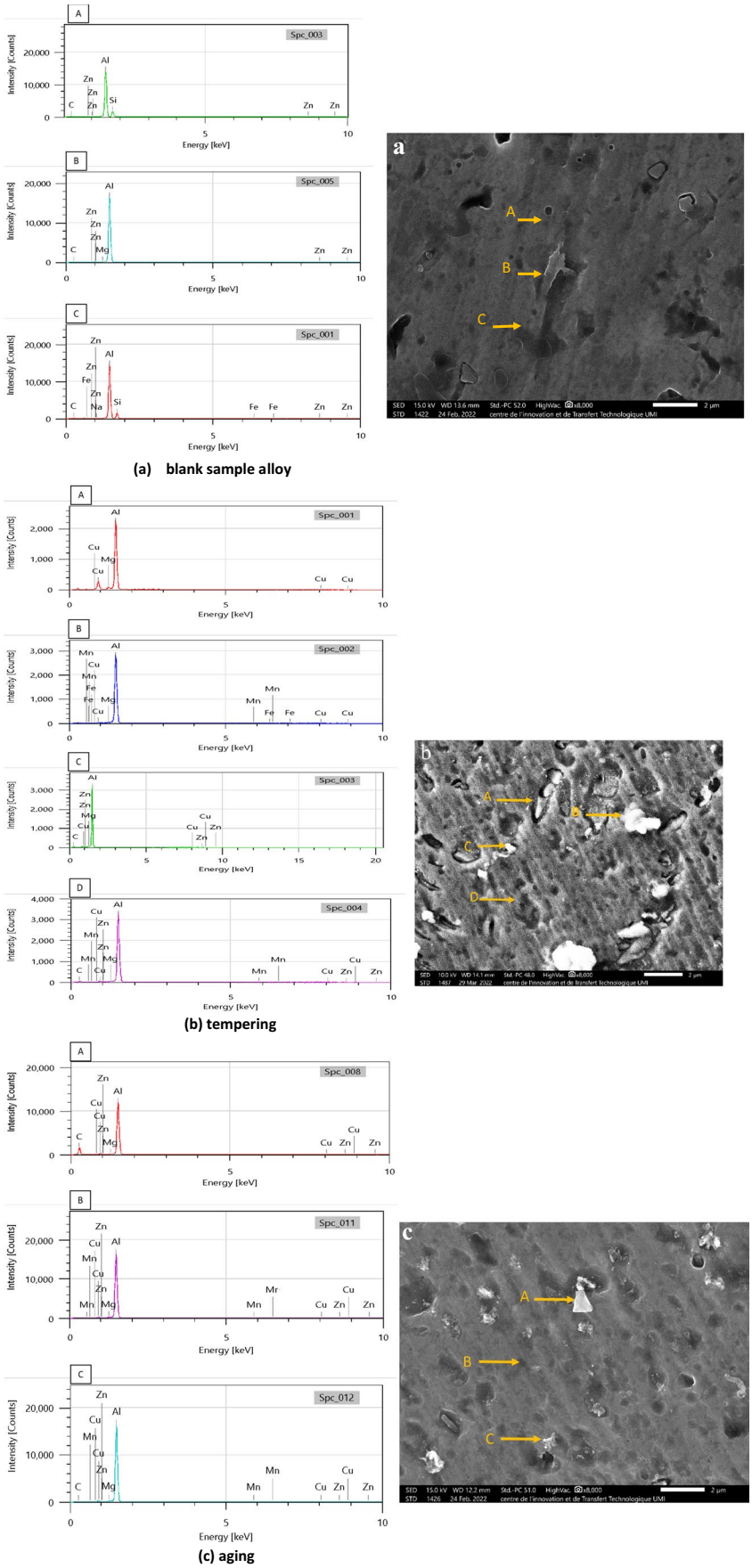

Fig. 4 EDS spectra of different zones in (**a**) blank sample alloy, (**b**) tempering, and (**c**) aging

$$\text{SSSS} \propto \rightarrow \text{ GP zones } \rightarrow \eta\, 0 \rightarrow \eta \quad (1)$$

where SSSSα represents a supersaturated solid solution,

GP zones are Guinier–Preston zones,η 0 is a metastable phase (with an Mg:Zn ratio in the range from 1:1 to 1:1.15),and η is a stable MgZn2 phase. MgZn2 plays the most significant role in the precipitate hardening process [35–37].

Figure 4 shows the change in hardness of AA7075 after quenching, followed by aging treatment.

3.2 Heat treatment effect on the microhardness of the AA7075

Figure 5 shows the hardness of six AA7075-T6 alloy samples: blank sample, tempering after 40 min at 475 °C, and one mature sample for 1 day, 2 days, 3 days, and 4 days. The test was submitted to a load force of 100 g for 15 s after polishing samples from 400 to 1200 grains and finishing polishing at 6 µm and 3 µm. The hardness tests were repeated at least ten times for each of the samples to calculate the average hardness of Vickers.

The average hardness results of AA7075-T6 alloy are shown in Fig. 5. The quenching heat treatment results in a significant decrease in hardness because of the formation of compounds and precipitated elements in the solid solutions, and the strength of the alloy increases, while a noticeable improvement in hardness can be observed in the maturation treatment after 4 days which is purely due to the formation of fine precipitates of the ή phase which are fully coherent or partially coherent. This partial coherence creates a stress field that hinders the dislocation increase in microhardness.

3.3 Fracture morphology

The SEM studied fracture characteristic of AA 7075-T6 alloy which underwent quenching treatment and aging treatment are presented in Fig. 6.

The control 7075-T6 aluminum alloy (A) fracture morphology displays high and low steps, tearing ridges with significant plastic deformations, large and small holes, and other mixed ductile and brittle fracture characteristics. After quenching, the alloy AA7075-T6 (B) exhibits a rise in the number of dimples, leading to the appearance of holes of various sizes. The number of dimples has increased when comparing Fig. 6 (C) and (A), which is related to the reduction in particle size and is consistent with the literature [21]. As these were the places of the nucleation of cavities, which can result in the formation of dimples, it suggests that the size and eventually the number of dimples are linked to the grain size and dislocations. Inferred from this is that older AA7075-T6 is less prone to rust than control AA7075-T6. Heat treatment can enhance the corrosion resilience of the metal. This is a result of the Al-Zn alloy's crystallization process, which can be summed up as follows:α (solution solide sursaturée solution) → zone G.P. → phase η′ (MgZn2) → phase η (MgZn2) [35, 36, 38].

The G.P. region, which contains Mg and Zn elements, is a spherical atomic segregation area. At the Al matrix's crystal surface, the cylindrical Mg and Zn atoms separate. The Al matrix and the Al matrix are identical. Phase η′ this is a

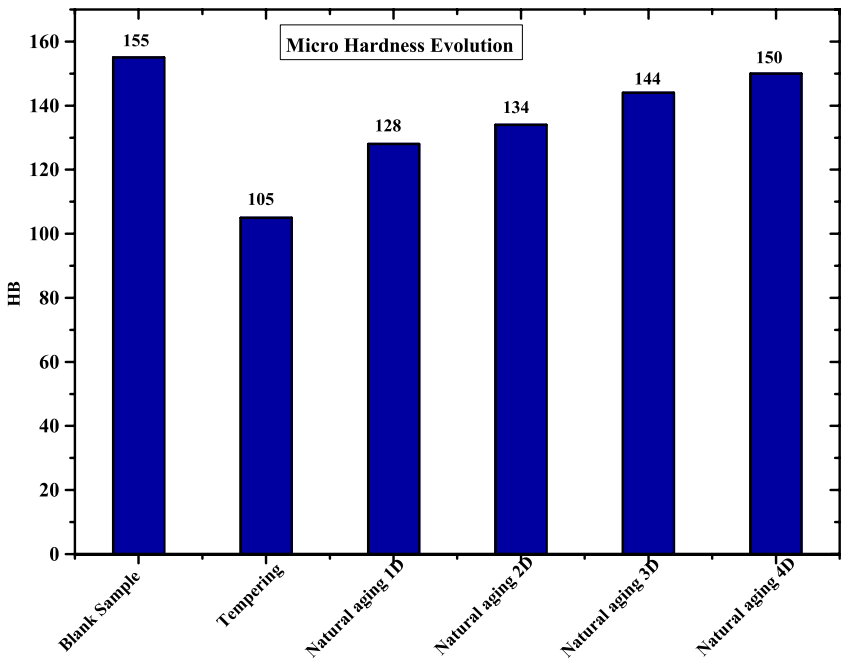

Fig. 5 Evolution of the hardness of the AA 7075-T6 blank sample alloy, tempering, and aging for 1 day, 2 days, 3 days, and 4 days

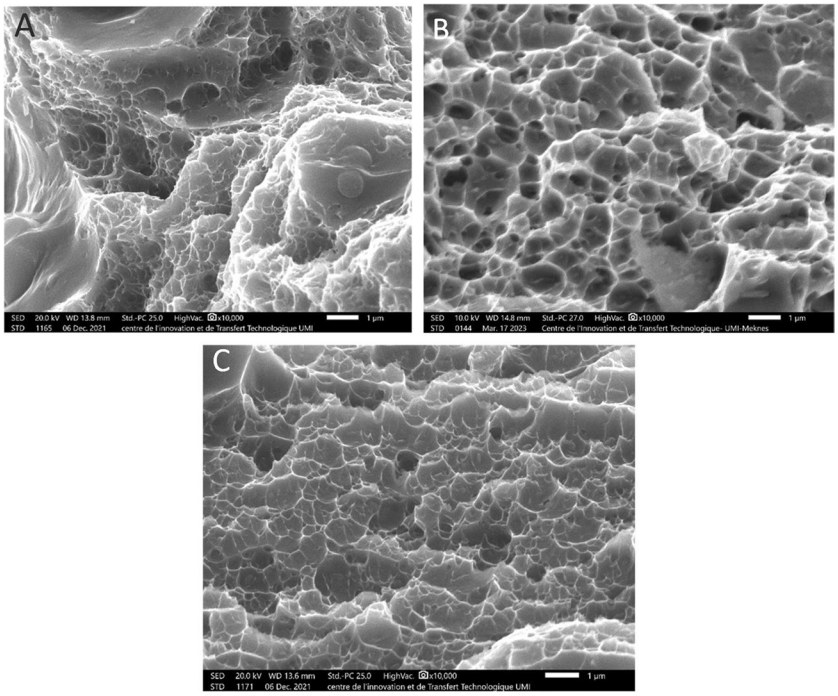

Fig. 6 SEM fractography of alloy specimens 7075-T6. (**A**) Blank sample alloy. (B) Tempering. (**C**) Aging

transitional phase made of MgZn2, which forms a full half-lattice in the matrix and has a hexagonal configuration in the Al matrix. The precipitation zone (PFZ), which grew noticeably bigger with the rise in grain size, is where the corrosion resistance ends. The alloy maintains its high toughness and strong corrosion protection as a consequence [39].

3.4 Tensile properties

The stress–strain curves of AA7075-T6 after different heat treatments are shown in Fig. 7.

Figure 7 illustrates the properties of the AA7075-T6 (A) alloy in the raw sample, including its tensile strength of 499 MPa, 462 MPa YS, and 13% elongation. 477.63 MPa UTS, 299.20 MPa YS, and 22.47% elongation for sample AA7075 (C), which has undergone aging, quenching of AA7075-T6(B) resulted in a 375 MPa reduction in tensile strength and an 18% increase in elongation. The control sample (A) exhibits the highest ultimate tensile and yield strengths, followed by sample (C), which received 5-day aging, and sample (B), which underwent rapid water cooling, according to the findings of the mechanical testing shown in Fig. 7. The other sample's grain sizes vary, which is the cause of the trend shown in their hardness and strength. This is consistent with Kenji et al.'s findings, which show that solid solution and grain refinement play a role in the hardening of Al–Mg alloys. Additionally, earlier research has demonstrated that materials with finer grains have more grain boundaries and are tougher and

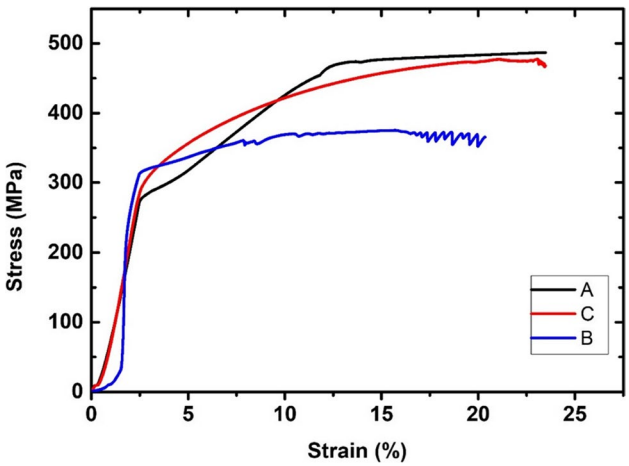

Fig. 7 Stress–strain curves of AA7075-T6 after different heat treatments. (**A**) Blank sample alloy. (**B**) Tempering. (**C**) Aging alloy

stronger than materials with coarser grains, which have fewer grain boundaries [40, 41]. Age-hardened materials are harder and stronger because there are more grain boundaries than samples that have undergone rapid cooling, which creates more barriers to dislocation migration during deformation. According to the Hall–Petch relationship, the yield stress *y* changes with grain size for the majority of materials [42]:

$$\sigma v = \sigma o + kyd1/2 \quad (2)$$

The terms *d*, *y*, and *ky* in this formula are constants specific to a certain material, and *d* is the average grain diameter. From a microstructural perspective, grain size's effect on yield strength and ultimate tensile strength may also be described. The number of restrictions increases with grain fineness. Slip or dislocation movement must occur across these grain boundaries during plastic deformation. A dislocation migrating from one polycrystalline grain to another must alter its direction of movement because the grain borders of polycrystalline grains have various crystallographic orientations. Both yield strength and ultimate tensile strength are increased as a result of these changes in direction, which also prevent dislocation movement. Age-hardened samples contain the most grain boundaries, which makes it more challenging for dislocations to migrate during plastic deformation. Because of this, age-hardened samples were shown to have the maximum yield strength and fracture toughness. Additionally, the 7075-T6 Al alloy employed in this study has 2% magnesium (Mg) and 6.2% zinc (Zn). Due to the production of MgZn2 precipitates in the structure during aging heat treatment, these two alloying elements contribute to a rise in the alloy's strength. The findings of Du et al., Li and Peng, Demir and Gündüz, and Kaya et al., who found that Al-Zn-Mg alloy can obtain the maximum degree of strength throughout both natural and artificial aging, are in agreement with this finding [46, 49].

3.5 Morphology of aluminum alloys after corrosion

The morphology of alloy AA 7075-T6 is shown in Fig. 8. The alloys were immersed for 126 h in the 50 g/L mass concentration NaCl solution in the salt spray, after we made a polishing of 400 to 1200 grains and a finishing polishing at 6 µm and 3 µm and then we made a chemical attack by the solution of KELLER.

SEM observed the surface of AA7075-T6 alloys after 126-h exposure to NaCl solution in salt spray. A general view of the microstructures of AA7075-T6 alloys is shown in Fig. 5 A, B, and C, respectively (A blank sample, B tempering, and C aging). The general analysis of the micrographs shows that the etching is randomly distributed on the three samples. For the AA7075-T6 alloy (A), the absence of pitting and formation of corrosion products around irregularly shaped precipitates and rods. For the quenched AA7075-T6 alloy (b), the formation of a significant number of pits and removal of most of the smaller precipitates from the sample surface by the etching. For the matured AA7075-T6 (C) formation of pits, they are less significant than the tempering treatment but we still have removed most of the small precipitates. The corrosion products continued to be concentrated mainly at the interface between the matrix and the larger intermetallic particles. We can also observe the corrosion products formed after the test have different sizes and shapes depending on the different treatments and the number of pits. We can also notice during the aging treatment, the pits are less significant compared to the tempering AA7075-T6 alloy and are absent in the blank sample AA7075-T6 alloy; this is a consequence of the corrosion resistance of the solid solution in the aging alloy.

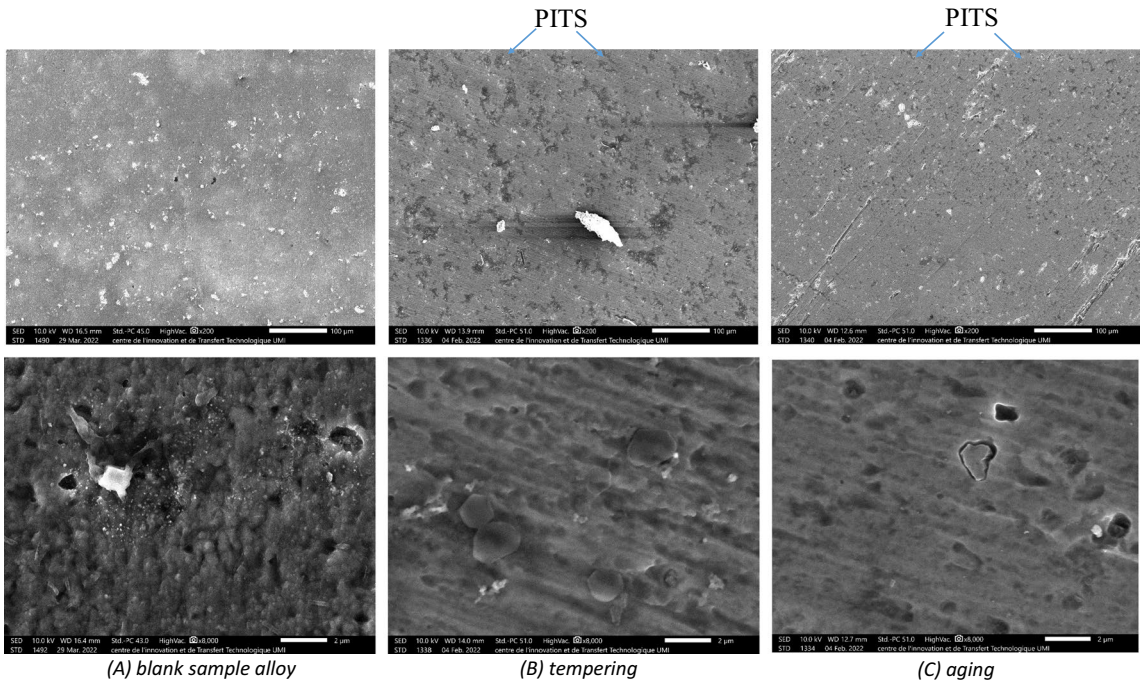

Fig. 8 SEM of different zones in (**A**) blank sample alloy, (**B**) tempering, and (**C**) aging after salt spray test

4 Conclusion

In this study, AA 7075-T6 specimens underwent quenching and aging heat treatments. The microstructure and mechanical tests such as tensile test and microhardness were examined. Here is a summary of the results:

1) The results show that heat treatment at a temperature of 470 °C has a significant impact on the transformation of the microstructure and mechanical microhardness of the resulting alloy. A remarkable 32.26% reduction in microhardness was achieved after quenching heat treatment, but a slight 3.23% decrease was observed during the 4-day aging treatment due to the formation of precipitated compounds and elements.
2) The formation of microsegregation weakens the 7075 aluminum alloy and subsequently has negative effects on its mechanical properties and application. The stress–strain curves of aged AA7075-T6 behaved well, but a significant reduction of 24.85% was observed for the quenched alloy.
3) A different microstructure by scanning electron microscopy was obtained after heat treatment before and after exposure to the salt spray test. The pitting was more severe for the quenching treatment than for the aging treatment and the control sample.

Author contribution All authors contributed to the design and development of the study. The preparation of the material, data collection, and analysis were carried out by Fatima Ezzohra El Garchani and Moulay Rachid Kabiri. The first draft of the manuscript was written by Fatima Ezzohra El Garchani, and all authors commented on the previous versions of the manuscript. All authors have read and approved the final manuscript.

Declarations

Competing interest The authors declare no competing interests.

References

1. Fuller C, Mahoney M, Calabrese M, Micona L (2010) Evolution of microstructure and mechanical properties in naturally aged 7050 and 7075 Al friction stir welds. Mater Sci Eng A 527:2233–2240. https://doi.org/10.1016/j.msea.2009.11.057
2. Bahrami M, Dehghani K, Givi MKB (2014) A novel approach to develop aluminum matrix nano-composite employing friction stir welding technique. Mater Des 53:217. https://doi.org/10.1016/j.matdes.2013.07.006
3. Vijaya Kumar P, Madhusudhan Reddy G, Srinivasa Rao K et al (2015) Microstructure and pitting corrosion of armor grade AA7075 aluminum alloy friction stir weld nugget zone—effect of post weld heat treatment and addition of boron carbide. Def Technol. 11(2):166–173. https://doi.org/10.1016/j.dt.2015.01.002
4. Gruenberg KM, Craig BA, Hillberry BM, Bucci RJ, Hinkle AJ et al (2004) Predicting fatigue life of pre-corroded 2024–T3 aluminum from breaking load tests. Int J Fatigue 26(6):615–627. https://doi.org/10.1016/j.ijfatigue.2003.10.010
5. Shi P, Mahadevan S (2003) Corrosion fatigue and multiple site damage reliability analysis. Int J Fatigue 25(6):457–469. https://doi.org/10.1016/S0142-1123(03)00020-3
6. Wang QY, Kawagoishi N, Chen Q (2003) Effect of pitting corrosion on very high cycle fatigue behavior. Scr Mater 49(7):711–716. https://doi.org/10.1016/S1359-6462(03)00365-8
7. DuQuesnay DL, Underhill PR, Britt HJ (2003) Fatigue crack growth from corrosion damage in 7075–T6511 aluminium alloy under aircraft loading. Int J Fatigue 25(5):371–377. https://doi.org/10.1016/S0142-1123(02)00168-8
8. Sankaran KK, Perez R, Jata KV (2001) Mater Sci Eng A 297:223–229
9. Pao PS, Feng CR, Gill SJ (2000) Corrosion fatigue crack initiation in aluminum alloys 7075 and 7050. Corrosion 56(10):1022–1031. https://doi.org/10.5006/1.3294379
10 Corrosion par piqure : S. Dey, M. K. Gunjan, Chattoraj (2008) "Effect of temper on the distribution of pits in AA7075 alloys", Corros. Sci, 50(10): 2895-2901, https://doi.org/10.1016/j.corsci.2008.07.015
11. Park JK, Ardell AJ (1983) Microstructures of the commercial 7075 Al alloy in the T651 and T7 tempers. Metall Trans A 14(10):1957–1965. https://doi.org/10.1007/BF02662363
12. Park JK, Ardell AJ (1988) Scr Metall 22:1115–1119
13. Bartges CW (1994) J Mater Sci Lett 13:776–778
14. Andreatta F, Terryn H, de Wit JHW (2003) Effect of solution heat treatment on galvanic coupling between intermetallics and matrix in AA7075-T6. Corros Sci 45(8):1733–1746. https://doi.org/10.1016/S0010-938X(03)00004-0
15. Wei RP, Liao C-M, Gao M (1998) A transmission electron microscopy study of constituent-particle-induced corrosion in 7075–T6 and 2024–T3 aluminum alloys. Metall Mater Trans A 29(4):1153–1160. https://doi.org/10.1007/s11661-998-0241-8
16. Dunford TG, Wilde (BE) (1987) In: M.E. Blum, P.M. French, R.M. Middleton, G.F. Vander Voort (Eds.), Microstructural Science, vol. 15, American Society for Metals and International Metallographic Society, 263
17. Wei RP, Liao C-M, Gao M (1998) A transmission electron microscopy study of constituent-particle-induced corrosion in 7075–T6 and 2024–T3 aluminum alloys. Metall Mater Trans A 29(4):1153–1160. https://doi.org/10.1007/s11661-998-0241-8
18. Metallic particle population in wrought aluminium alloys during ingot casting and thermo-mechanical processing". Mater Sci Forum, 331 43-154, 2000, https://doi.org/10.4028/www.scientific.net/MSF.331-337.143.
19. Gao M, Feng CR, Wei RP (1998) An analytical electron microscopy study of constituent particles in commercial 7075–T6 and 2024–T3 alloys. Metall Mater Trans A 29(4):1145–1151. https://doi.org/10.1007/s11661-998-0240-9
20. Andreatta F, Terryn H, de Wit JHW (2004) Corrosion behaviour of different tempers of AA7075 aluminium alloy. Electrochimica Acta 49(1):2851–2862. https://doi.org/10.1016/j.electacta.2004.01.046.2
21 Orłowska M et al (2022) The influence of heat treatment on the mechanical properties and corrosion resistance of the ultrafine-grained AA7075 obtained by hydrostatic extrusion. Materials 15(12):4343. https://doi.org/10.3390/ma15124343
22. "Fine-grained AA 7075 processed by different thermo-mechanical processings - ScienceDirect". https://www.sciencedirect.com/science/article/abs/pii/S0921509314011319. (Consulted May 29, 2023)

23. Wang G, Gu Z, Yu G, Li X (2022) Precipitates evolution of the AA7075-H18 alloy sheet during the application of the solution heat treatment process. Mater Lett 318:132230. https://doi.org/10.1016/j.matlet.2022.132230
24 Clark R et al (2005) On the correlation of mechanical and physical properties of 7075–T6 Al alloy. Eng Fail Anal 12(4):520–526. https://doi.org/10.1016/j.engfailanal.2004.09.005
25. Liu Y, Mol JMC, Janssen GCAM (2016) "Combined corrosion and wear of aluminium alloy 7075-T6". J Bio Tribo Corros, 2(2), https://doi.org/10.1007/s40735-016-0042-3.
26. "B557 Standard test methods for tension testing wrought and cast aluminum- and magnesium-alloy products". https://www.astm.org/b0557-15.html. (Consulted May 29, 2023)
27. D Desjardins, R Oltra (1998) Corrosion sous contrainte Phénoménologie et mécanismes Bombannes 1990. Les Editions de physique.
28 Jedrychowski M, Tarasiuk J, Bacroix B, Wronski S (2013) Electron backscatter diffraction investigation of local misorientations and orientation gradients in connection with evolution of grain boundary structures in deformed and annealed zirconium. A new approach in grain boundary analysis. J Appl Crystallogr 46:483–92
29. Kamp N, Sinclair I, Starink MJ (2002) Toughness-strength relations in the overaged 7449 al-based alloy. Metall Mater Trans A 33(4):1125–1136. https://doi.org/10.1007/s11661-002-0214-2
30. Isadare AD, Aremo B, Adeoye MO, Olawale OJ, Shittu MD (2023) Effect of heat treatment on some mechanical properties of 7075 aluminium alloy. Mat Res 16:190–194. https://doi.org/10.1590/S1516-14392012005000167
31 Berg LK et al (2001) GP-zones in Al–Zn–Mg alloys and their role in artificial aging. Acta Mater 49(17):3443–3451. https://doi.org/10.1016/S1359-6454(01)00251-8
32. Li XZ, Hansen V, GjØnnes J, Wallenberg LR (1999) HREM study and structure modeling of the η· phase, the hardening precipitates in commercial Al-Zn-Mg alloys. Acta Mater 47:2651–2659. https://doi.org/10.1016/S1359-6454(99)00138-X
33 Huang ZW, Loretto MH, Smallman RE, White J (1996) The mechanism of nucleation and precipitation in 7075–0.7 Li alloy. Acta Metall. Mater. 42(2):549–559. https://doi.org/10.1016/0956-7151(94)90509-6
34. M Orłowska et al (2022) "The influence of heat treatment on the mechanical properties andcorrosion resistance of the ultrafine-grained AA7075 obtained by hydrostatic extrusion". Materials, 15(12). https://doi.org/10.3390/ma15124343.
35. Xu X, Liu D, Zhang X, Liu C, Liu D, Ma A (2020) Effects of ultrasonic surface rolling on the localized corrosion behavior of 7B50-T7751 aluminum alloy. Materials 13(3):738. https://doi.org/10.3390/ma13030738
36. R Su, Y Qu, X Li, J You, R Li (2016) "Effect of retrogression and reaging on stress corrosion cracking of spray formed Al Alloy". Mater Sci Appl., 7(1), https://doi.org/10.4236/msa.2016.71001.
37 Rout PK, Ghosh MM, Ghosh KS (2015) Influence of aging treatments on alterations of microstructural features and stress corrosion cracking behavior of an Al-Zn-Mg Alloy. J Mater Eng Perform. 24:2792–2805. https://doi.org/10.1007/s11665-015-1559-1
38. Zhao X, Chen X, Wang X (2018) Effect of aging processes on corrosion behavior and stress corrosion sensitivity of pre-stretched 7075 aluminum alloy. Mater Corros 69(7):850–857
39. Kaneko K, Hata T, Tokunaga T, Horita Z (2009) Fabrication and characterization of supersaturated Al-Mg alloys by severe plastic deformation and their mechanical properties. Mater Trans 50(1):76–81. https://doi.org/10.2320/matertrans.MD200813
40. "(PDF) friction stir welding of a commercial 7075-T6 aluminum alloy: grain refinement, Thermal Stability and Tensile Properties". https://www.researchgate.net/publication/266016588_Friction_Stir_Welding_of_a_Commercial_7075-T6_Aluminum_Alloy_Grain_Refinement_Thermal_Stability_and_Tensile_Properties. (Consulted May 29, 2023)
41. RB Figueiredo, TG Langdon (2009) "Using severe plastic deformation for the processing of advanced engineering materials". Mater Trans, 50(7).
42. Li J, Peng Z, Li C, Peng QZ, Chen W, Zheng Z (2008) Mechanical properties, corrosion behaviors and microstructures of 7075 aluminium alloy with various aging treatments. Trans Nonferrous Metals Soc China 18:755–762. https://doi.org/10.1016/S1003-6326(08)60130-2
43. "Quantitative evaluation of precipitates in an Al–Zn–Mg–Cu alloy after isothermal aging | Request PDF". https://www.researchgate.net/publication/248495746_Quantitative_evaluation_of_precipitates_in_an_Al-Zn-Mg-Cu_alloy_after_isothermal_aging. (Consulted May 29, 2023)
44. H Kaya (2012) "The effect of aging on the machinability of AA7075 aluminium alloy", Scientific Research and Essays, 7, https://doi.org/10.5897/SRE12.411.